euspen's 23rd International Conference & Exhibition, Copenhagen, DK, June 2023
www.euspen.eu

Design and validation of a Cryogenic Active Vibration Isolator

A.M. Albers[1], B.C.T. van Bree[1], S.L. Paalvast[1], D.P.P. Struver[2], J.P.M.B. Vermeulen[2], H.L.M.M. Janssen[1]

[1] JPE, Maastricht-Airport, The Netherlands
[2] Eindhoven University of Technology, Control Systems Design - Mechatronic Systems Design, Eindhoven, The Netherlands

richard.albers@jpe.nl

Abstract

This paper describes the design principle and validation of a single axis cryogenic active vibration isolator (CAVI). The CAVI can be placed as a module in a parallel kinematic configuration for vibration isolation in multiple translational degrees of freedom (Tx,Ty,Tz). The CAVI is designed to operate within a gravitational-wave observatory [1]. The operating environment is at cryogenic temperatures of < 10 K and ultra-high vacuum conditions of $< 10^{-9}$ mbar. Within this application, the CAVI is used to attenuate both floor vibrations and direct force disturbances affecting the isolation platform and attached payload. Main source of vibrations are the cryopumps used to achieve the cryogenic temperatures. The cut-off frequency for vibration isolation must be less than one Hertz.

The isolation performance both depends on passive and active features. For this isolator, these features include standard mass-spring-damper suspension as passive feature and the use of a seismometer and a voice coil placed within a servo-loop to provide additional isolation as an active feature [2]. The seismometer is a custom made element, sensing the displacement between a seismic- and payload mass using an interferometer at nanometer resolution while the seismic mass is suspended at a low eigenfrequency. A cryogenic compatible voice coil actuator is used for force actuation, creating compensation forces onto the payload platform [3]. For active isolation, feedback control is being used: next to proportional action, additional local lag- and lead effect filters have been used to stabilize the control loop and define the damping of the closed-loop resonance.

Initial setup and -testing showed that the cut-off frequency for vibration isolation is decreased from 10 Hz in passive mode down to 0.5 Hz in active mode. The resulting dynamic rms displacement of the vibration on an example cryostat cold-plate, which is a typical disturbance source for this application, is decreased from 6.5 µm measured on the cold-plate to 0.5 µm when using the active vibration isolation.

Keywords: precision engineering, mechatronics, vibration isolation, inertial sensing, voice coil actuator, ultra high vacuum, cryogenic

1. Introduction

One of the key challenges for the gravitational-wave observatory, called Einstein Telescope [1], is to keep the optical mirrors, which must detect gravitational waves, free from vibrations. Next to the seismic isolation of an individual optical mirror, additional vibration isolation must be used on the thermal connection up to the mirror as well. As requirement for the isolation performance, it must provide a cut-off frequency of at most one Hertz with a goal of 0.1 Hz in multiple translational degrees of freedom. Since the mirror must be connected with thermal braids for cooling down to a few Kelvin, vibrations caused by cryopumps are introduced through these connections. To mitigate the introduction of these vibrations, the idea is to isolate a cooled body, a so called "Cold Finger", as a final cold spot which is thermally connected to the mirror. This "Cold Finger" must be isolated from floor vibrations and vibrations from the connected cooling system as well. To accomplish this, a Cryogenic Active Vibration Isolator (CAVI) is devised.

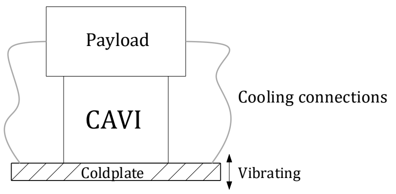

Figure 1. Use case: the Cryogenic Active Vibration Isolator (CAVI) used between payload and cold plate of a cryo cooling system.

2. Concept

The concept of a Tx, Ty, Tz cryogenic active vibration isolator is based on a parallel kinematic combination of three individual modules. For the ongoing description within this paper, operation and performance of a single module is discussed, providing isolation in a single translational degree-of-freedom only. For impression, module dimensions are (l×w×h): 67 mm × 83 mm × 72 mm.

Each module is equipped with a payload mass and an inertial sensor mass, both suspended in series by using monolithic flexures. This principle is depicted in figure 2.

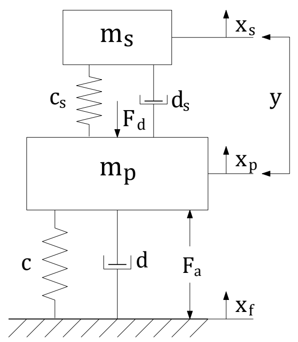

Figure 2. Basic passive isolation is performed by using suspension elements c,d and m_p. An additional inertial measurement facilitated by sensor suspension elements c_s, d_s and m_s.

By accurately measuring the relative displacement *y* between the two masses m_p and m_s, a quantity for the displacement of the payload mass m_p is obtained after a certain threshold frequency. By using this information *y* in combination with a voice coil actuator providing a force F_a onto the payload mass m_p, feedback control can be implemented. In effect, the isolation frequency can be improved to sub-Hz level compared to a few Hz for an equivalent passive isolation system. In addition, the magnitude of the effective closed-loop resonance can be minimized. Both the attenuation of floor vibrations and the rejection of direct disturbances to the payload can be significantly improved by making the isolation active.

2.1. Inertial sensing principle

A custom made inertial sensor is integrated within the isolator that both acts as accelerometer and seismometer over specific frequency ranges. The frequency ranges are separated by the mechanical eigenfrequency of the inertial sensor suspension: $\omega_0 = \sqrt{\frac{c_s}{m_s}}$.
Sensing modes can be described by input acceleration and by input displacement at the payload mass as respectively:

$$T_{\ddot{x}_p y}(s) = \frac{Y(s)}{\ddot{X}_p(s)} = \frac{-m_s}{m_s s^2 + d_s s + c_s}$$

$$T_{x_p y}(s) = \frac{Y(s)}{X_p(s)} = \frac{-m_s s^2}{m_s s^2 + d_s s + c_s}$$

For frequencies below the eigenfrequency, the output *y* observes acceleration with frequency-independent sensitivity (flatline). Sensitivity of the acceleration mode within this frequency range is the relation $\frac{1}{{\omega_0}^2} = \frac{m_s}{c_s}$. Above the eigenfrequency, the output *y* observes displacement of m_p with frequency-independent sensitivity. The sensitivity of the displacement mode is unity. These modes of sensing are shown in figure 3.

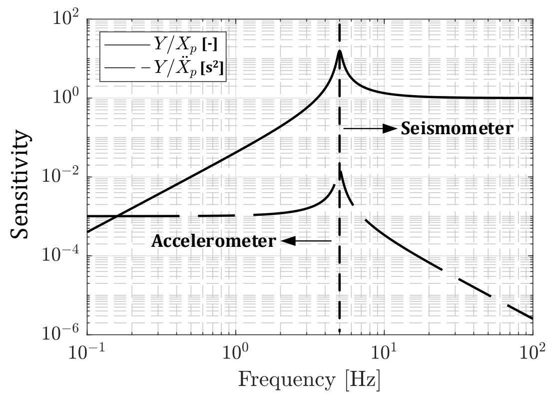

Figure 3. Inertial sensing can be differentiated in an accelerometer and a seismometer mode.

To create maximum sensitivity for the acceleration mode to output displacement, the suspension eigenfrequency must be as low as possible. To achieve this low eigenfrequency, the suspension stiffness is designed to be as low as possible and the sensor mass as high as possible within the available volume.

As a drawback created by the low suspension stiffness, Gravity Compensation (GC) must be applied to compensate the introduced sag of the inertial mass within the direction of gravity. By doing so, no additional positive stiffness must be introduced as this affects the already minimized suspension eigenfrequency. Therefore it has been chosen to apply magnetic GC (MGC) instead by using permanent magnets. The MGC concept is depicted in figure 4. The MGC can be adjusted to meet the desired operating point for achieving maximum symmetric range for displacement of m_s. The total available moving range of m_s is only two millimeter.

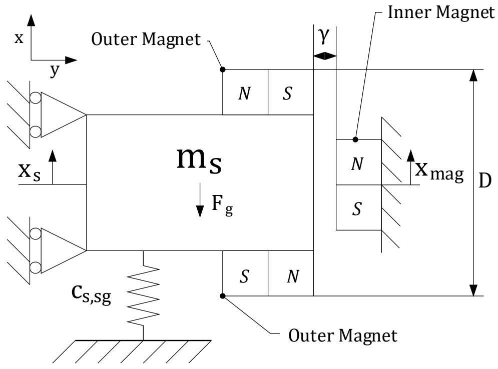

Figure 4. Gravity force F_g compensation on inertial mass m_s by using permanent magnets.

Advantage of the MGC is that it creates extra negative stiffness at the operating point as can be seen in Figure 5. The combined decreased stiffness from both suspension and MGC is favorable as it decreases the eigenfrequency of the seismometer suspension.

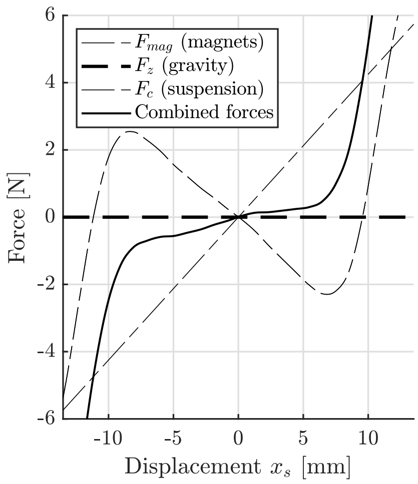

Figure 5. By adding negative stiffness provided by the magnets, the combined stiffness is advantageous in the operating point at around zero displacement.

The displacement *y* is measured by using an interferometer at nanometer resolution with sufficient bandwidth. The static value of *y* is also used as feedback to set the MGC within the mid-range operating point to enable maximum symmetric range.

2.2. Actuator

The actuator providing force F_a is a custom made ultra-high-vacuum and cryogenic compatible voice coil actuator [3].

2.3. Control

The displacement *y* between the payload- and inertial mass is actively controlled to zero to achieve additional standstill of the payload mass m_p within a desired frequency range. Feedback control is implemented by using the signal *y* as input and F_a as ouput depicted in figure 2.

A control structure with the identifiable disturbance inputs is depicted in figure 6.

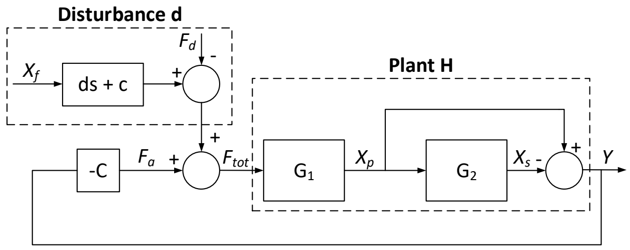

Figure 6. Control loop with disturbance inputs floor vibrations X_f and direct payload force disturbance F_d

Based on figure 2 and figure 6, the plant H can be expressed as:

$$G_1(s) = \frac{X_p}{F_{tot}} = \frac{1}{m_p s^2 + ds + c + (1 - G_2)(d_s s + c_s)}$$

$$G_2(s) = \frac{X_s}{X_p} = \frac{d_s s + c_s}{m_s s^2 + d_s s + c_s}$$

$$H(s) = \frac{Y}{F_{tot}} = G_1(1 - G_2)$$

When evaluating the plant tranfer H from F_a to y, a passband characteristic can be identified (Figure 7). First eigenmode is the sensor suspension at 4 Hz, the second eigenmode is the payload suspension at 8 Hz.

Control strategy is focussed on extending the isolation bandwidth with a minimized magnitude of the closed-loop resonance. Passband action must be maintained from below 1 Hz to above 8 Hz. To guarantee stability, local lag action is added below 4 Hz and local lead action above 8 Hz. Proportional gain is chosen such that any parasitic effects do not jeopordize stability or performance. The description of controller C can be expressed as:

$$C(s) = K\left(\frac{1}{4} \cdot \frac{s + 2\pi \cdot f_{lag} \cdot 2}{s + 2\pi \cdot f_{lag}/2}\right)\left(9 \cdot \frac{s + 2\pi \cdot f_{lead}/3}{s + 2\pi \cdot f_{lead} \cdot 3}\right)$$

With K the proportional gain, f_{lag} the center frequency providing local lag action and f_{lead} the center frequency providing local lead action. The frequency response figures of the open-loop transfer CH is depicted in figure 7 and figure 8.

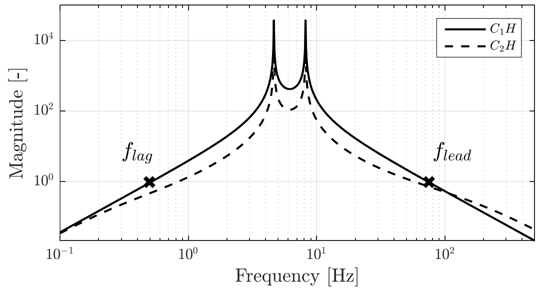

Figure 7. Bode magnitude plot of open-loop transfers with C_1H using only proportional control, and C_2H using additional compensation with local lead- and lag effect filters. Using a pole-zero around f_{lag} and a zero-pole around f_{lead} respectively.

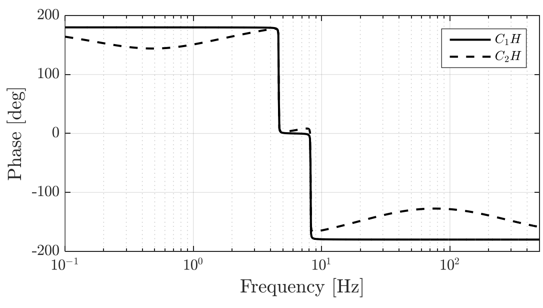

Figure 8. Bode phase plot of open-loop transfers C_1H and C_2H

3. Disturbance transmissibility

Disturbance transmissibility can be differentiated in disturbance caused by floor vibrations X_f and disturbance caused by direct interaction of forces Fd onto the payload. Based on figure 2 and figure 6, the individual transmissibility for floor disturbance and payload disturbance can be expressed as:

$$\frac{X_p}{X_f} = \frac{G_1(ds + c)}{1 + CG_1(1 - G_2)}$$

$$\frac{X_p}{F_d} = \frac{-G_1}{1 + CG_1(1 - G_2)}$$

In figure 9, the resulting transmissibility of floor vibration to payload displacement is shown. In figure 10, the transmissibility of payload disturbance forces to payload displacement is shown. Within both figures, both passive- and active isolation of the module is shown.

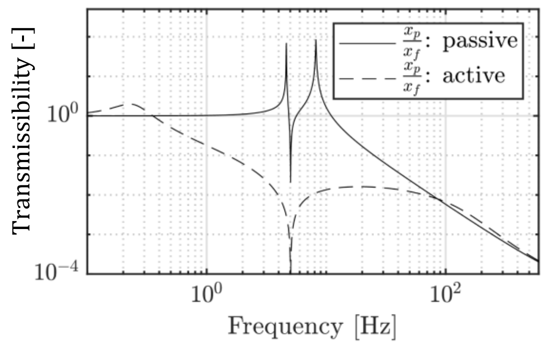

Figure 9. Disturbance transmissibility from floor- to payload displacement

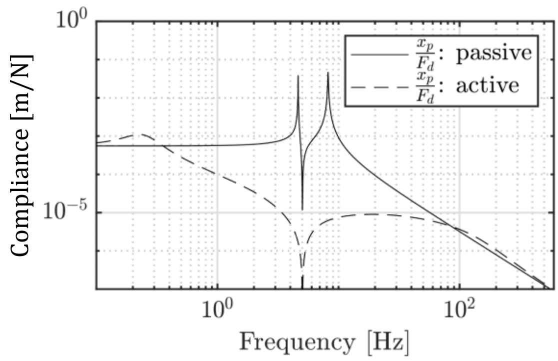

Figure 10. Disturbance transmissibility from payload disturbance force to payload displacement

As can be seen: passive isolation starts at 10 Hz whereas active isolation starts at 0.33 Hz. The magnitude of the closed-loop resonance: Q-factor, is decreased significantly compared to the dominant resonances present in the passive isolator. In passive isolation the Q-factor is roughly 100, in active state the Q-factor results in 2.

4. Validation of transmissibility

Once the demonstrator for the CAVI has been built and configured correctly, the transmissibility from floor displacement to payload displacement has been validated by experiment. By using a vibration source: a shaker, located at the base of the vibration isolator, the transmissibility is determined by measuring the individual displacement of both the shaker and the payload against a quiete reference. As can be seen in figure 11, the transmissibility for both the passive- and active state of the vibration isolator is shown. Reflecting back to figure 4, it can be concluded that the real world transmissibility mismatches the theoretical performance of the isolator slightly. The eigenfrequency of the dominant mode and parasitic mode appear to be swapped for the passive isolator. Active isolation starts at roughly 0.5 Hz. Within the validation, a limited bandwidth from 0.1 Hz to 50 Hz is used to quantify the transmissibility

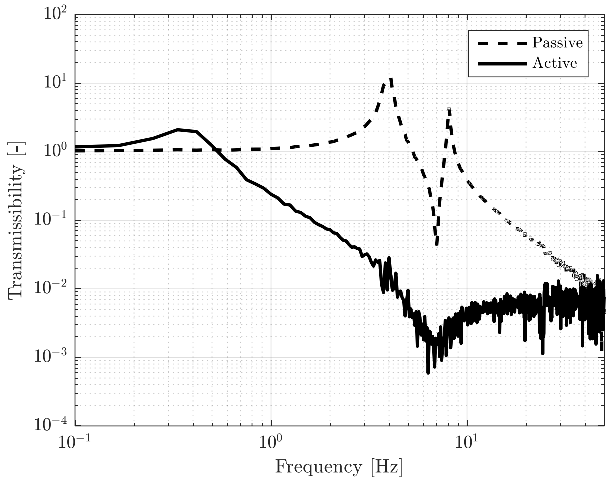

Figure 11. Transmissibility of vibration isolator from floor displacement to payload displacement. In frequency range from 0.1 Hz to 50 Hz.

5. Isolation performance

The isolation performance was measured with the vibration isolation placed on a cryostat cold-plate but under atmospheric- and room temperature conditions. An external displacement sensor was used to qualify displacements of the payload mass. The cold-plate introduces the typical vibrations that would be present within the application due to the presence of a closed-cycle cryopump; a mechanical refrigerator that introduces a periodic distortion to the signal. The example cold-plate used, typically generates a 2 Hz fundamental frequency and additional harmonics. The measurement on isolation performance is performed in both passive- and active mode. As a reference, also the vibrations directly on the cold-plate are measured. These measurements are depicted within the cumulative power spectrum density (CPSD) plot in figure 12.

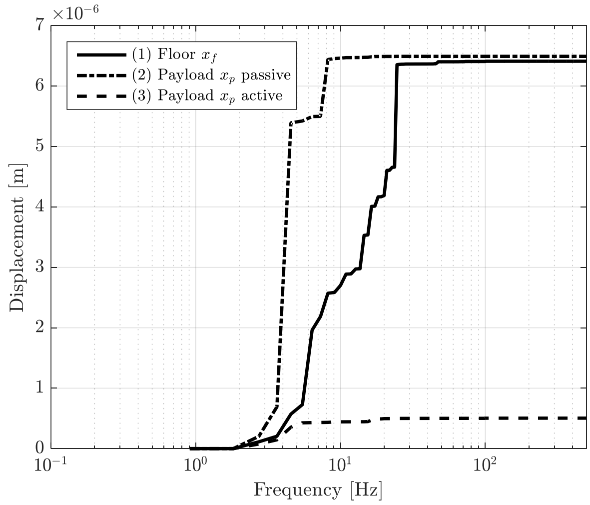

Figure 12. Square root of CPSD: the floor displacement, payload with passive vibration isolation, and payload with active vibration isolation.

As can be seen in the CPSD, most significant contribution in floor vibration (1) is below 30 Hz. Measuring roughly 6.5 µm rms displacement up to 200 Hz. When using passive isolation (2), there is no advantage in rms result given the example excitation by the cold-plate. Contributions above 10 Hz are attenuated by the passive isolation. Significant contribution in case using the isolator passively is caused by the second harmonic generated by the cryocooler-vibration that excites the first eigenmode of the vibration isolator at 4 Hz. When using the vibration isolator actively (3), effective displacement is decreased to 0.5 µm: a factor 13 decrease in effective displacement when using the example cryostat for input disturbance generation.

6. Future work

Some improvements can be made to the current design of this vibration isolator.

1) Crosstalk between the voice coil actuator and the magnetic gravity compensation exists. This limits active control at sub-Hertz frequencies. Eliminating this crosstalk creates ability to decrease the isolation cut-off frequency even further.
2) The magnetic gravity compensation mechanism cannot compensate gravity forces of the inertial mass within direction of gravity. Redesign of this mechanism must be performed without altering the suspension frequency significantly.
3) In perspective of costs, the used interferometer for the inertial sensor is considered too expensive. Alternatives must be considered without jeopardising resolution and bandwidth too much.
4) Mismatch in theoretical model and real-world identification should be investigated.

Within the discussed application: the gravitational-wave telescope, the presented module will be used as part of a three translational degrees of freedom isolation platform, isolating floor vibrations and platform disturbances in Tx,Ty,Tz. The individual modules will be placed in a parallel kinematic configuration. An impression of this multiple degrees of freedom isolation platform is shown in figure 13.

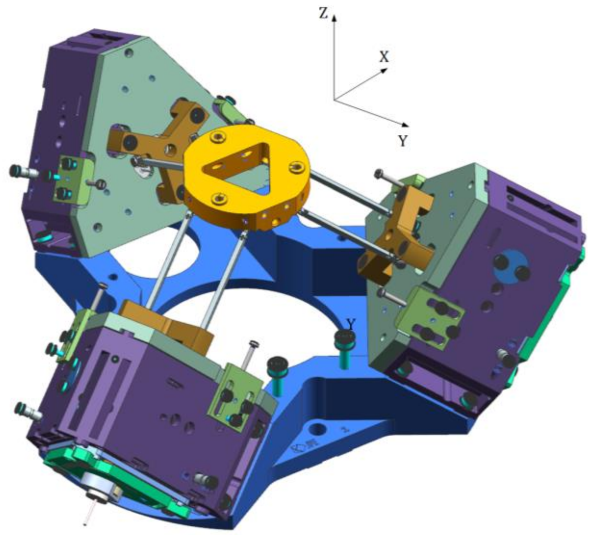

Figure 13. Multiple translational degrees of freedom isolation platform Tx,Ty,Tz, using three Cryogenic Active Vibration Isolators.

References

[1] Einstein Telescope, Website Einstein Telescope." (2021), http://www.et-gw.eu

[2] Design of a voice coil actuated active vibration isolator for cryogenic conditions, master thesis, D.P.P. Struver, (2022)

[3] JPE B.V. https://www.jpe- innovations.com